Artif Life Robotics
DOI 10.1007/s10015-014-0186-5

ORIGINAL ARTICLE

Comparison of proportional-derivative and active-force controls on vibration of a flexible single-link manipulator using finite-element method

Abdul Kadir Muhammad · Shingo Okamoto · Jae Hoon Lee

Received: 8 April 2014 / Accepted: 10 October 2014

Abstract The purposes of this research are to derive the equations of motion of a flexible single-link system by a finite-element method, to develop the computational codes in order to perform dynamics simulations with vibration control and to propose an effective control scheme of a flexible single-link manipulator using two control strategies, namely proportional-derivative (PD) and active-force (AF) controls. The flexible manipulator used in this paper consists of an aluminum beam as a flexible link, a clamp-part, a servo motor to rotate the link, and a piezoelectric actuator to control vibration. Computational codes on time history responses, FFT (Fast Fourier Transform) processing, and eigenvalues–eigenvectors analysis were developed to calculate the dynamic behavior of the link. Furthermore, the PD and AF control strategies were designed and compared their performances through the calculations. The calculated results show the superiority of the proposed AF control comparing the PD one to suppress the vibration of the flexible single-link manipulator.

This work was presented in part at the 19th International Symposium on Artificial Life and Robotics, Beppu, Oita, January 22-24, 2014.

A. K. Muhammad (✉) · S. Okamoto · J. H. Lee
Graduate School of Science and Engineering, Ehime University, Matsuyama, Japan
e-mail: y861008b@mails.cc.ehime-u.ac.jp

S. Okamoto
e-mail: okamoto.shingo.mh@ehime-u.ac.jp

J. H. Lee
e-mail: jhlee@ehime-u.ac.jp

A. K. Muhammad
Mechanical Engineering Department, State Polytechnic of Ujung Pandang, Makassar, Indonesia

Keywords Active-force control · Finite-element method · Flexible manipulator · Vibration control

1 Introduction

Employment of flexible manipulators is recommended in the space and industrial applications in order to accomplish high performance requirements such as high-speed besides safe operation, increasing of positioning accuracy, and lower energy consumption, namely less weight. However, it is not usually easy to control a flexible manipulator because of its inheriting flexibility. Deformation of the flexible manipulator when it is operated must be considered by any control. Its controller system should be dealt with not only its motion but also vibration due to the flexibility of the link.

In the past few decades, a number of modeling methods and control strategies using piezoelectric actuators to deal with the vibration problem have been investigated by researchers [1–4]. Nishidome and Kajiwara [1] investigated a way to enhance performances of motion and vibration of a flexible-link mechanism. They used a modeling method based on modal analysis using the finite-element method. The model was described as a state space form. Their control system was constructed with a designed dynamic compensator based on the mixed of H_2/H_∞. They recommended separating the motion and vibration controls of the system. Yavus Yaman et al. [2] and Kircali et al. [3] studied an active vibration control technique on aluminum beam modeled in cantilevered configuration. The studies used the ANSYS package program for modeling. They investigated the effect of element selection in finite-element modeling. The model was reduced to state space form suitable for application of H_∞ [2] and spatial H_∞ [3] controllers to suppress vibration of

Published online: 27 November 2014

the beam. They showed the effectiveness of their techniques through simulation. Zhang et al. [4] have studied a flexible piezoelectric cantilever beam. The model of the beam using finite-elements was built by ANSYS application. Based on the Linear Quadratic Gauss (LQG) control method, they introduced a procedure to suppress the vibration of the beam with the piezoelectric sensors and actuators were symmetrically collocated on both sides of the beam. Their simulation results showed the effectiveness of the method.

Furthermore, applications of the AF control strategy to suppress vibration of a flexible system were done by some researchers [5–7]. Hewit et al. [5] used the AF control for deformation and disturbance attenuation of a flexible manipulator. Then, a PD control was used for trajectory tracking of the flexible manipulator. They used a motor as an actuator. Modeling of the manipulator was done using virtual link coordinate system (VLCS). Their simulation results had shown that the proposed control could cancel the disturbance satisfactorily. Tavakolvour et al. [6] investigated the AF control application for a flexible thin plate. Modeling of their system was done using finite-difference method. Their calculated results showed the effectiveness of the proposed controller to reduce vibration of the plate. Tavakolvour and Mailah [7] studied the AF control application for a flexible beam with an electromagnetic actuator. Modeling of the beam was done using finite-difference method. The effectiveness of the proposed controller was confirmed through simulation and experiment.

The purposes of this research are to derive the equations of motion of a flexible single-link system by a finite-element method, to develop the computational codes in order to perform dynamics simulations with vibration control and to propose an effective control scheme of a flexible single-link manipulator using two control strategies, namely proportional-derivative (PD) and active-force (AF) controls. The flexible manipulator used in this paper consists of an aluminum beam as a flexible link, a clamp-part, a servo motor to rotate the link, and a piezoelectric actuator to control vibration. Computational codes on time history responses, FFT (Fast Fourier Transform) processing, and eigenvalues–eigenvectors analysis were developed to calculate the dynamic behavior of the link. An end-effector that treated as a concentrated mass was introduced to demonstrate a complete flexible single-link manipulator system. Furthermore, the PD and AF control strategies were designed to suppress the vibration. It was done by adding bending moments generated by the piezoelectric actuator to the single link. Finally, their performances were compared through the calculations.

2 Formulation by the finite-element method

Figure 1 shows the position vector $\boldsymbol{r}$ of an arbitrary point P in the link in the global and rotating coordinate frames. Let

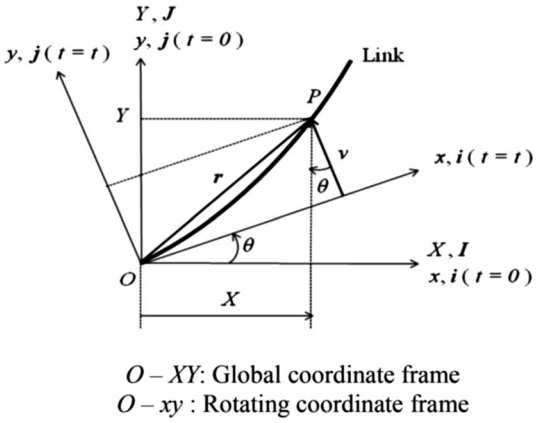

Fig. 1 Position vector of an arbitrary point P in the link in the global and rotating coordinate frames

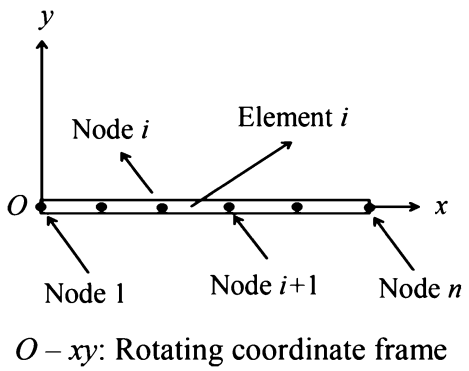

Fig. 2 Rotating coordinate frame and the link divided by the one-dimensional and two-node elements

the link as a flexible beam has a motion that is confined in the horizontal plane as shown in Fig. 1. The O–XY frame is the global coordinate frame while O–xy is the rotating coordinate frame fixed to the root of the link (z-axis is fixed). The unit vectors in X, Y, x, and y axes are denoted by $\boldsymbol{I}$, $\boldsymbol{J}$, $\boldsymbol{i}$, and $\boldsymbol{j}$, respectively. A motor is installed on the root of the link. The rotational angle of the motor when the link rotates is denoted by $\theta(t)$. The velocity vector of the arbitrary point P in the link at time $t = t$, shown in Fig. 1, is expressed by

$$\dot{\boldsymbol{r}}\,(x,\ t) = \dot{X}(x,\ t)\,\boldsymbol{I} + \dot{Y}(x,\ t)\,\boldsymbol{J}. \tag{1}$$

The link has been discretized by finite elements [8]. Every finite element (Element i-th) has two nodes namely Node i and Node $(i + 1)$. Every node (Node i) has two degrees of freedom, namely the lateral deformation $v_i(t)$ and the rotational angle $\psi_i(t)$. The length, the cross-sectional area, and the area moment of inertia around z-axis of the i-th element are denoted by l_i, S_i, and I_{zi}, respectively. Mechanical properties of every element are denoted as Young's modulus E_i and mass density ρ_i.

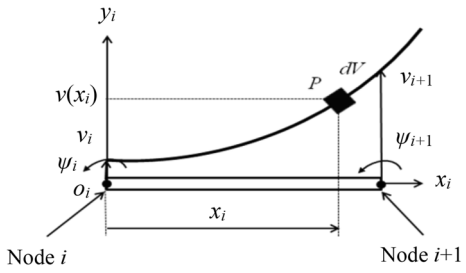

Fig. 3 Element coordinate frame of the i-th element

Figure 2 shows the rotating coordinate frame and the link divided by one-dimensional and two-node elements. Then, Fig. 3 shows the element coordinate frame of the i-th element and an arbitrary point P in the i-th element. Here, there are four boundary conditions together at nodes i and $(i+1)$ when the one-dimensional and two-node element is used. The four boundary conditions are expressed as nodal vector as follows:

$$\boldsymbol{\delta}_i \;=\; \left\{ v_i \;\; \psi_i \;\; v_{i+1} \;\; \psi_{i+1} \right\}^T. \tag{2}$$

Then, the hypothesized deformation has four constants as follows: [9]

$$v_i = a_1 \;+\; a_2 x_i \;+\; a_3 x_i^2 \;+\; a_4 x_i^3, \tag{3}$$

where x_i is position coordinate of the arbitrary point P in the x_i-axis of the element coordinate frame. Then, the relation between the lateral deformation v_i and the rotational angle ψ_i of the Node i is given by

$$\psi_i = \frac{\partial v_i}{\partial x_i}. \tag{4}$$

Moreover, from mechanics of materials, the strain of Node i can be defined by

$$\varepsilon_i = -y_i \frac{\partial^2 v_i}{\partial x_i^2}, \tag{5}$$

where y_i is position coordinate of the arbitrary point P in the y_i-axis of the element coordinate frame.

Furthermore, substituting derivation of Eqs. (1), (2), (4) to the general expressions for kinetic energy and strain energy of a finite element, respectively, then applying to Lagrange's equation, so the equation of motion of the i-th element can be obtained as follows:

$$\boldsymbol{M}_i \ddot{\boldsymbol{\delta}}_i + \boldsymbol{C}_i \dot{\boldsymbol{\delta}}_i \;+\; \left[\boldsymbol{K}_i - \dot{\theta}^2(t)\; \boldsymbol{M}_i \right] \boldsymbol{\delta}_i = \ddot{\theta}(t)\, \boldsymbol{f}_i \,, \tag{6}$$

where $\boldsymbol{M}_i$, $\boldsymbol{C}_i$, $\boldsymbol{K}_i$, and $\ddot{\theta}(t)\, \boldsymbol{f}_i$ are the mass matrix, damping matrix, stiffness matrix, and the excitation force generated by the rotation of the motor, respectively. The matrices and vector in Eq. (6) are represented as

$$\boldsymbol{M}_i \;=\; \frac{\rho_i S_i l_i}{420} \begin{bmatrix} 156 & 22l_i & 54 & -13l_i \\ 22l_i & 4l_i^2 & 13l_i & -3l_i^2 \\ 54 & 13l_i & 156 & -22l_i \\ -13l_i & -3l_i^2 & -22l_i & 4l_i^2 \end{bmatrix} \tag{7}$$

$$\boldsymbol{K}_i = \frac{E_i I_{z_i}}{l_i^3} \begin{bmatrix} 12 & 6l_i & -12 & 6l_i \\ 6l_i & 4l_i^2 & -6l_i & 2l_i^2 \\ -12 & -6l_i & 12 & -6l_i \\ 6l_i & 2l_i^2 & -6l_i & 4l_i^2 \end{bmatrix} \tag{8}$$

$$\mathbf{C}_i = \alpha \mathbf{K}_i \tag{9}$$

$$\boldsymbol{f}_i \;=\; \frac{\rho_i S_i l_i}{60} \left\{ 30 l_{1-i} + 9 l_i, \;\; 5 l_{1-i} l_i + 2 l_i^2, \;\; 21 l_i, \;\; -5 l_{1-i} l_i + 3 l_i^2 \right\}^T. \tag{10}$$

The length of the i-th element, the length from Element 1 to i, and the Rayleigh damping factor are denoted by l_i, l_{1-i}, and α [9], respectively.

Finally, the equation of motion of the system with n elements considering the boundary conditions is given by

$$\boldsymbol{M}_n \ddot{\boldsymbol{\delta}}_n \;+\; \boldsymbol{C}_n \dot{\boldsymbol{\delta}}_n + \left[\boldsymbol{K}_n - \dot{\theta}^2(t)\; \boldsymbol{M}_n \right] \boldsymbol{\delta}_n = \ddot{\theta}(t)\, \boldsymbol{f}_n \,. \tag{11}$$

3 Modeling

In this paper, we defined and used two types of computational models of the single-link manipulator.

3.1 Model *A*

A model of the single–link manipulator, the clamp-part, and the piezoelectric actuator were defined as Model *A*. Figure 4a shows Model *A*. The link including the clamp-part and actuator was discretized by 22 elements. The clamp-part is more rigid than the link. Therefore, Young's modulus of the clamp-part was set in 1,000 times of the link's. The piezoelectric actuator was bonded to a one-side surface of element 2. A schematic representation on modeling of the piezoelectric actuator is shown in Fig. 5. Furthermore, a strain gage was bonded to the position of Node 3 of the single link (0.11 m from the origin). Physical parameters of the single-link model and the piezoelectric actuator are shown in Table 1.

The piezoelectric actuator suppresses the vibration of the single-link flexible manipulator by adding bending moments at nodes 2 and 3 of the single-link, M_2 and M_3. The bending moments are generated by applying voltages E to the piezoelectric actuator as shown in Fig. 5. The bending moments proportional to the voltages which are expressed by

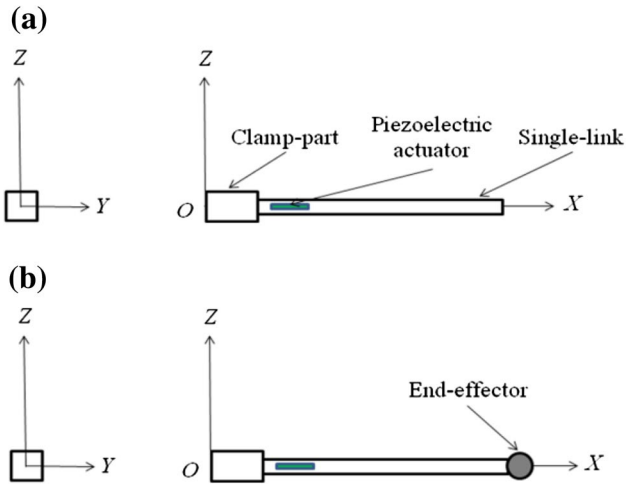

Fig. 4 Computational models of the single-link manipulator **a** Model *A* single-link with piezoelectric actuator **b** Model *B* single-link with piezoelectric actuator and end-effector

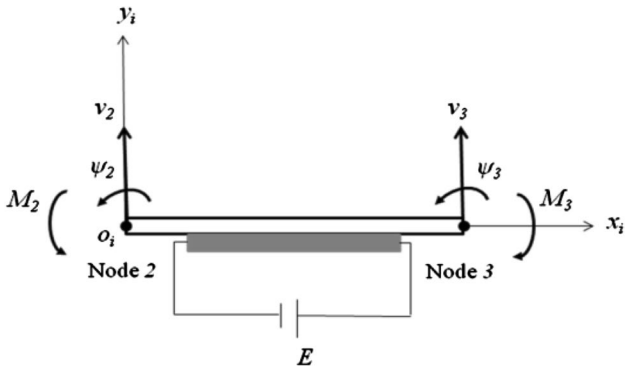

Fig. 5 Modeling of piezoelectric actuator (*top view*)

$$M_2 = -M_3 = d_1 E. \tag{12}$$

Here d_1 is a constant quantity and M_2 opposites to M_3.

Furthermore, the voltage to generate the bending moments is proportional to the strain ε of the single link due to the vibration. The relation can be expressed as follows:

$$E = \pm \frac{1}{d_2}\varepsilon. \tag{13}$$

Here d_2 is a constant quantity. Then, d_1 and d_2 will be determined by comparing the calculated results and experimental ones.

3.2 Model *B*

Figure 4b shows Model *B* that an end-effector of the single-link manipulator is considered. Model *B* is used to show that the proposed control strategies are also suitable for such system. The end-effector is presented by adding a concentrated mass to the previous model. Therefore, the kinetic energy of the tip element was increased due to the concentrated mass.

Applying the kinetic energy and the strain energy to Lagrange's equation, so the equation of motion of the tip element containing the concentrated mass is given by

$$\begin{aligned}&[\boldsymbol{M}_i + \boldsymbol{M}_{icm}]\,\ddot{\boldsymbol{\delta}}_i + C_i\dot{\boldsymbol{\delta}}_i \\ &+\left[\boldsymbol{K}_i - \dot{\theta}^2(t)\,(\boldsymbol{M}_i + \boldsymbol{M}_{icm})\right]\boldsymbol{\delta}_i = \ddot{\theta}(t)\,\{\boldsymbol{f}_i + \boldsymbol{f}_{icm}\},\end{aligned} \tag{14}$$

where the vector of f_{icm} is given by

$$\boldsymbol{f}_{icm} = -m_c\left\{0\ 0\ l_{1-i} + l_i\ 0\right\}^T, \tag{15}$$

Table 1 Physical parameters of the single-link and the piezoelectric actuators

l Total length	m	3.91×10^{-1}
l_l Length of the link	m	3.50×10^{-1}
l_c Length of the clamp-part	m	4.10×10^{-2}
l_a Length of the actuator	m	2.00×10^{-2}
S_l Cross section area of the link	m^2	1.95×10^{-5}
S_c Cross section area of the clamp-part	m^2	8.09×10^{-4}
S_a Cross section area of the actuator	m^2	1.58×10^{-5}
I_{zl} Cross section area moment of inertia around z-axis of the link	m^4	2.75×10^{-12}
I_{zc} Cross section area moment of inertia around z-axis of the clamp-part	m^4	3.06×10^{-8}
I_{za} Cross section area moment of inertia around z-axis of the actuator	m^4	1.61×10^{-11}
E_l Young's Modulus of the link	GPa	7.03×10^{1}
E_c Young's Modulus of the clamp-part	GPa	7.00×10^{4}
E_a Young's Modulus of the actuator	GPa	4.40×10^{1}
ρ_l Density of the link	kg/m^3	2.68×10^{3}
ρ_c Density of the clamp-part	kg/m^3	9.50×10^{2}
ρ_a Density of the actuator	kg/m^3	3.33×10^{3}
α Damping factor of the link	–	2.50×10^{-4}

and the concentrated mass matrix M_{icm} can be expressed as

$$\boldsymbol{M}_{icm} = \begin{bmatrix} 0 & 0 & 0 & 0 \\ 0 & 0 & 0 & 0 \\ 0 & 0 & m_c & 0 \\ 0 & 0 & 0 & 0 \end{bmatrix}, \tag{16}$$

where m_c is the mass of the concentrated mass.

3.3 Validation of formulation and computational codes

Computational codes were developed to perform dynamics simulation of the system based on the formulation that explained above. The validation was done using time history response analysis of free vibration, natural frequencies using FFT (Fast Fourier Transform) processing, vibration modes and natural frequencies using eigenvalues–eigenvectors analysis and time history response analysis due to the excitation force [8].

4 Control scheme and simulations

4.1 Control scheme

A control scheme to suppress the vibration of the single link was designed using the piezoelectric actuator. It was done by adding bending moments generated by the piezoelectric actuator to the single link. Therefore, the equation of motion of the system become

$$\boldsymbol{M}_n\ddot{\boldsymbol{\delta}}_n + \boldsymbol{C}_n\dot{\boldsymbol{\delta}}_n + \left[\boldsymbol{K}_n - \dot{\theta}^2(t)\,\boldsymbol{M}_n\right]\boldsymbol{\delta}_n = \ddot{\theta}(t)\boldsymbol{f}_n + \boldsymbol{u}_n(t), \tag{17}$$

where the vector of $\boldsymbol{u}_n(t)$ containing M_2 and M_3 is the control force generated by the actuator to the single link.

To drive the actuator, two different control strategies namely PD and active-force controls have been designed and examined. Their performances were compared through calculation.

4.1.1 Proportional-derivative control

Substituting Eqs. (13)–(12) gives

$$M_2, M_3 = \pm \frac{d_1}{d_2}\varepsilon. \tag{18}$$

Based on Eq. (17), the bending moment can be defined in s-domain as follows:

$$\boldsymbol{U}_n(s) = \boldsymbol{G}_C(s)\ \ (\varepsilon_d(s) - \varepsilon_3(s)), \tag{19}$$

where ε_d and ε_3 denote the desired and measured strains at Node 3, respectively. The bending moment in Eq. (19) will be applied to Node 2 and 3 according to the position

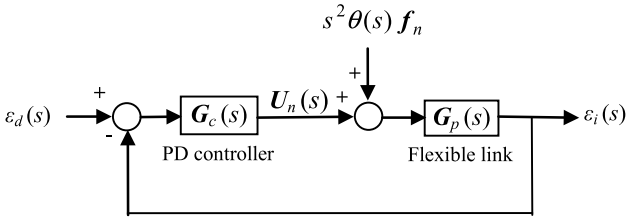

ε_d: Desired strain, ε_i: Measured strains at Node i
θ: Rotation angle of the motor, $\boldsymbol{U}_n$: Applied bending moment

Fig. 6 Block diagram of PD control of the flexible manipulator

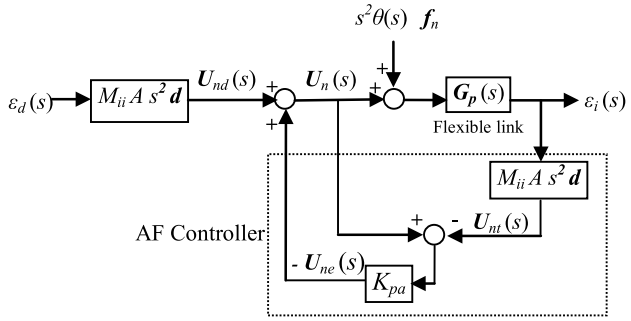

ε_d: Desired strain, ε_i: Measured strains at Node i
θ: Rotation angle of the motor, M_{ii}: Component of mass matrix
A: Conversion from ε_i to v_i, $\boldsymbol{d}$: Position vector
$\boldsymbol{U}_{nd}$: Desired bending moment, $\boldsymbol{U}_n$: Applied bending moment
$\boldsymbol{U}_{ne}$: Excitation bending moment, $\boldsymbol{U}_{ne}$: Bending moment

Fig. 7 Block diagram of AF control of the flexible manipulator

of the piezoelectric actuator; therefore configuration of the PD controller can be written by a vector in s-domain as follows:

$$\boldsymbol{G}_C(s) = \left\{0\ 0\ 0\ K_p + K_d\,s\ 0\ -\left(K_p + K_d\,s\right)\ 0\ \cdots\ 0\right\}^T, \tag{20}$$

where K_p and K_d are proportional and derivative gains of the PD controller, respectively.

Moreover, transfer function of the n elements flexible link $\boldsymbol{G}_p(s)$ can be obtained by substituting Eq. (5) to Eq. (17) and transferred to s-domain using Laplace's transform. A block diagram of the PD control strategy for the single-link system is shown in Fig. 6.

4.1.2 Active-force control

Figure 7 shows the block diagram of the AF control that is proposed in this research. In this strategy, vibration of the system is controlled by canceling the excitation bending moment. The following steps are the way to estimate and cancel the excitation bending moments.

Firstly, the strain, ε_3 at Node 3 is measured to estimate the lateral deformation, v_3 at the Node 3. Based on the mechanics of materials, the relation between the strain and the lateral deformation can be defined as follows:

$$\frac{v_3}{\varepsilon_3} = -\frac{x^2(x-3l)}{6y(x-l)} = A, \tag{21}$$

where l, x, and y are the length of the link and the position of Node 3 in x and y directions, respectively.

Secondly, the actual force in the s-domain acting at Node 3 can be defined in the form of the Newton's equation of motion as follows:

$$F_3(s) = M_{33}\, s^2\, v_3, \tag{22}$$

where M_{33} is the component of the mass matrix corresponding to Node 3.

Thirdly, the bending moments acting at Nodes 2 and 3 are estimated using the following equation:

$$\boldsymbol{U}_{nt}(s) = \pm F_3(s)\,\boldsymbol{d}. \tag{23}$$

The vector $\boldsymbol{d}$ that represents the position vector from the reference point to the position where the excitation force acting can be written as follows:

$$\boldsymbol{d} = \{0\ 0\ 0\ l_2\ 0\ l_2\ 0 \cdots\ 0\}^T. \tag{24}$$

Fourthly, based on Fig. 6, the excitation bending moments can be calculated as

$$\boldsymbol{U}_{ne}(s) = K_{pa}\,\{\boldsymbol{U}_{nt}(s) - \boldsymbol{U}_n(s)\}, \tag{25}$$

where K_{pa} is the non-dimensional proportional gain of the proposed AF control.

Finally, the bending moment applying as a control force to control the vibration of the system can be calculated as follows:

$$\boldsymbol{U}_n(s) = -\boldsymbol{U}_{ne}(s) + \boldsymbol{U}_{nd}(s), \tag{26}$$

where $\boldsymbol{U}_{nd}(s)$ is the desired bending moment which is zero.

The negative of $\boldsymbol{U}_{ne}(s)$ indicates that the bending moment is used to cancel the vibration of the system.

4.2 Calculated results

The time history responses of strains at Node 3 in the controlled system were calculated for Models A and B as shown in Fig. 4a, b. The concentrated mass, m_c, used as the end-effector is 0.005 (kg).

Examining several gains of the PD and AF controls leaded to $K_p = 600$ (Nm), $K_d = 0.005$ (Nms), and $K_{pa} = 0.83$ (–) as the better ones. Figures 8 and 9 show the uncontrolled and controlled time history responses for Models A and B, respectively. They were calculated when the motor rotated by the angle of $\pi/2$ radians (90°) in 0.68 (s). The maximum strain of uncontrolled system for Model A was 452.50×10^{-6}. Using PD and AF controllers, the maximum strain became 168.00×10^{-6} and 86.50×10^{-6}, respectively, as shown in Fig. 8. The maximum strains of uncontrolled system for Model B were 907.00×10^{-6}. Using PD and AF controllers, the maximum strain became 277.00×10^{-6} and 148.00×10^{-6}, respectively, as shown in Fig. 9.

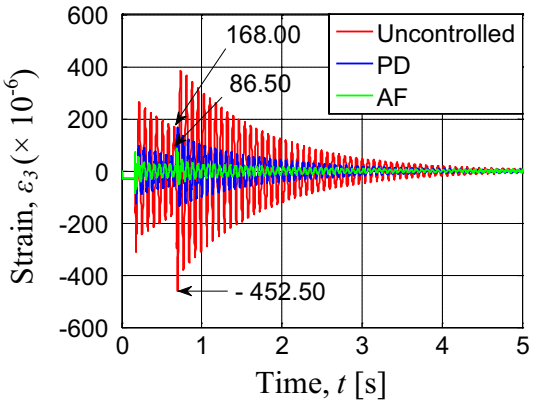

Fig. 8 Calculated time history responses of strains at Node 3 for uncontrolled and controlled Model A due to the excitation force generated by the motor's rotation [$K_p = 600$ (Nm), $K_d = 0.005$ (Nms), and $K_{pa} = 0.83$ (–)]

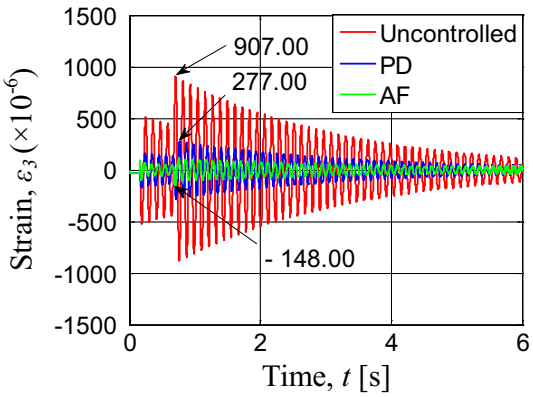

Fig. 9 Calculated time history responses of strains at Node 3 for uncontrolled and controlled Model B due to the excitation force generated by the motor's rotation [$m_c = 0.005$ (kg), $K_p = 600$ (Nm), $K_d = 0.005$ (Nms), and $K_{pa} = 0.83$ (–)]

It was verified from these results that the vibration of the flexible single-link manipulator can be more effectively suppressed using the proposed AF controller compared to the PD one.

5 Conclusion

The equation of motion for the flexible single-link manipulator had been derived using the finite-element method.

Computational codes had been developed in order to perform dynamics simulations of the system. The validities of the formulation, computational codes, and modeling of the system were shown by examining the experimental and calculated results on time history responses, natural frequencies, and vibration modes. The proportional-derivative (PD) and active-force (AF) control strategies were designed to drive the actuator. Their performances were compared through the calculations. The calculated results show the superiority of the proposed AF control comparing PD one to suppress the vibration of the flexible single-link manipulator.

References

1. Nishidome C, Kajiwara I (2003) Motion and vibration control of flexible-link mechanism with smart structure. JSME Int J 46(2):565–571
2. Yaman Y et al (2001) Active vibration control of a smart beam. In: Proceedings of the 2001 CANSMART symposium, 2001, pp 125–134
3. Kircali OF et al (2009) Active vibration control of a smart beam by using a spatial approach. In: New Developments in Robotics, Automation and Control, Chap 21. In Tech, pp 378–410
4. Zhang J et al (2010) Active vibration control of piezoelectric intelligent structures. J Comput 5(3):401–409
5. Hewit JR et al (1997) Active force control of a flexible manipulator by distal feedback. Mech Mach Theory 32(5):583–596
6. Tavakolpour AR et al (2011) Modeling and simulation of a novel active vibration control system for a flexible structures. WSEAS Trans Syst Control 6:184–195
7. Tavakolpour AR, Mailah M (2012) Control of resonance phenomenon in flexible structures via active support. J Sound Vib 331:3451–3465
8. Muhammad AK et al (2014) Computer simulations on vibration control of a flexible single-link manipulator using finite-element method. In: Proceeding of 19th International Symposium of Artificial Life and Robotics. pp 381–386
9. Lalanne M et al (1983) Mechanical Vibration for Engineers. Wiley, New York